Photothermal circular dichroism studies of single nanoparticles

Späth, P.R.

4

Correlated optical and TEM measurements of quasi achiral and "superchiral" gold nanoparticles

Chemically synthesized chiral nanoparticles have strong chiral features and show strong circular dichroism (CD). However, a chemical synthesis process typically goes along with nonuniformity of shape and size, thereby affecting the chiroptical properties of the individual particles in the ensemble of synthesized particles. To find a clear relation between geometrical chirality and their chiroptical response, a correlative structural and optical study is essential on a single-particle level. Most existing single-particle circular dichroism measurements based on transmission or dark-field microscopy do not allow for a highly sensitive detection of the chiroptical response. We have shown that our photothermal circular dichroism (PT-CD) microscope is capable of detecting CD signals of single chiral nanoparticles down to g-factors of 3×10^{-4}*. Here we combine PT-CD measurements with electron tomography (ET) to investigate the relation between geometrical chiral features and chiroptical response of wet-chemically synthesized chiral nanorods and quasi-spherical gold nanospheres at the single-particle level. By analyzing their 3D structures, obtained from ET, we find that the synthesized chiral particles indeed have geometric features that give rise to a biased chiroptical response which is also confirmed by single-particle optical measurements. In addition, single-particle optical measurements show that the particles have a broad distribution in their strength and handedness of the chiroptical response. Particles with strong chiral features of a certain handedness exhibit a clear bias in their CD signal, however, the strength of their CDs is not directly related to the strength of the geometric chirality. To study how plasmonic resonance effects could play a role, we performed boundary-element method (BEM) simulation considering the 3D structures of the particles directly obtained from tomography without smoothing structural features.*

4.1. Introduction

A molecule or nanoobject is chiral when it cannot be superimposed with its mirror image. The standard way of detecting chiral nanoobjects is by measuring their circular dichroism (CD) spectra using a commercial CD spectrometer. CD is the differential absorption of left and right circularly polarized light. A commercial CD spectrometer measures the CD spectra, via extinction, of an ensemble of molecules and particles averaging out heterogeneous single-molecule/particle information. Several research groups have developed single-particle circular dichroism techniques [1–4], however, they do not measure a true absorption signal and are lacking sensitivity. Photothermal circular dichroism microscopy (PT-CD) is capable of measuring the direct differential absorption, free from scattering contributions [5] and can measure CD on single nanoparticles with unprecedented sensitivity [6]. In PT-CD we use Koehler illumination for the heating beam, because it preserves the polarization state of light in the focal plane, while, we use a highly focused probe beam which keeps the spatial resolution to the diffraction limit. For measurements of single chiral metallic nanoparticles, the leakage of linear dichroism (LD) into CD needs to be rejected to obtain CD sensitivity down to g-factor of 10^{-3} and smaller. We have shown in chapter 3 that, by employing a dual modulation of the polarization, the leakage of LD into CD can be rejected with a rejection ratio of more than 300 [6], which allows us to investigate small CD values in rod-like particles. The high detection sensitivity and rejection of artefacts is promising to study various chiral nanoparticles at the single-particle level.

Chiral plasmonic nanoparticles have recently received much attention owing to their potential in light manipulation as for example in circular polarizers [7], enantiomeric sensing of biomolecules [8], chiral waveguides [9] or negative refractive index materials [10]. Bottom-up fabricated plasmonic nanoparticles can be tailor-made with specific optical properties [11], however, their fabrication process is difficult for up-scaling. In addition, the polycrsytallinity of nanofabricated structures can dampen their plasmonic properties [12]. Chemically synthesized plasmonic nanoparticles are single-crystalline and can also exhibit strong CD. Due to the wet-chemical synthetic process their production can be upscaled easily. However, precisely controlling their shape and hence their chiral features remains a difficult task. A recent study [13] could reveal the correlation between the shape and the chiroptical response in chemically synthesized particles. This study relied on the reconstruction of the 3D shape of the nanoparticles by performing ET. The reconstruction was used to detect features of geometric chirality that lead to the strong chiroptical response of the particles. By applying fast Fourier transformations (FFTs) on the reconstructed nanoparticles, González-Rubio and coworkers [13] identified that repetitive wrinkles, i.e. helical features, caused the strong chirality in these systems. However, the study of such complex particles not only requires the knowledge of the shape of the particles but also the chiroptical response at the single-particle level. Until now most studies of the optical properties of chiral nanoparticles are carried out in ensemble measurements for the lack of sensitive single-particle CD techniques. Here we combine optical PT-CD measurements with ET to correlate geometrical features of chiral nanoparticles to optical CD at the single-particle level. Two types of nanoparticles are used in this study - chemically synthesized chiral gold nanorods and quasi-spherical gold nanospheres. Chiral nanorods are prepared by micelle-directed growth on top of gold nanorods [13]. Chiral molecules in the nanorod's solution

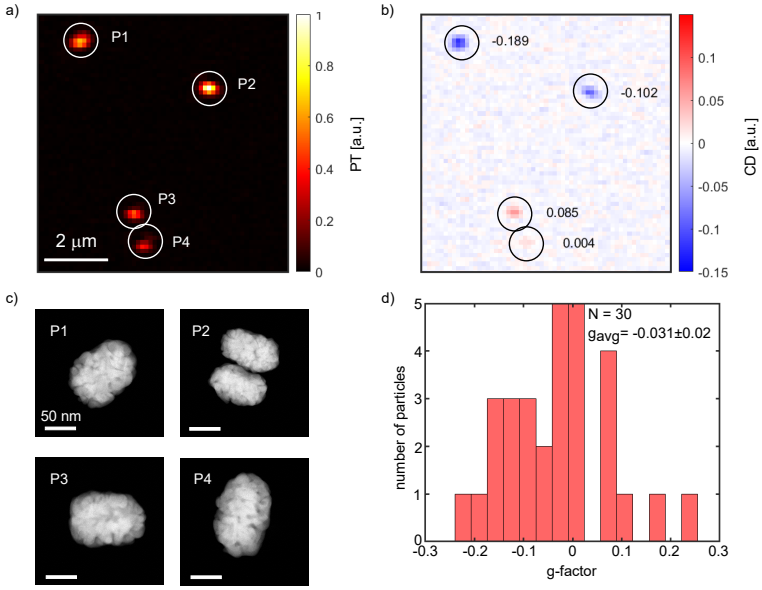

Figure 4.1: (a) Photothermal and (b) circular dichroism images of three single and one dimer of chiral gold nanorods. (c) TEM images of three single and one dimer of nanorods as labelled in (a). The scale bars are 50 nm. (d) Histogram of g-factors of 30 single chiral gold nanorods.

form worm-like micelles that can stick on top of the nanorods' surface and help in transferring chirality to the rod by further deposition of metal atoms. Gold nanospheres bought from Nanocomposix are single-crystalline nanoparticles with a truncated octahedral shape which is supported by transmission electron microscopy (TEM) measurements. To investigate the chiroptical properties of single nanoparticles, we dropcasted a solution of nanoparticles on a TEM grid where we can perform both, optical and TEM measurements.

4.2. Results and discussion

4.2.1. Chiral nanorods

Figure 4.1 (a) and (b) show photothermal (PT) and PT-CD images of four chiral nanoparticles. Correlated TEM measurements in (c) show that three of these particles are single nanorods and one is a dimer. The presence of a dimer is evidenced by the PT signal, which is about twice that of a single-particle. The absorption anisotropy (g-factor) of the ensemble was determined by means of commercial CD spectrometer as $g \sim$ -0.015 (see figure S4.1 in the SI) at the wavelength of the PT measurements (660 nm). The single-particle measurements in figure 4.1 reveal a striking difference with the ensemble measurements, namely that not only the strength of CD of individual particles varies strongly, also its sign can vary. We find that individual particles can have substantially stronger CD response as compared to the ensemble measurements, however, as the sign of CD also varies, the overall chiroptical

response of the ensemble is drastically reduced in magnitude. To check whether the PT-CD measurements resemble the chiroptical behaviour of the ensemble technique we performed more PT-CD measurements, all correlated with TEM measurements. Figure 4.1 (d) shows the histogram of g-factors of 30 chiral nanorods obtained by PT-CD at $660\,\mathrm{nm}$. Our single-particle measurements yield an average g-factor of -0.031$\pm$ 0.02, which is on the same order of magnitude as the ensemble measurements ($g \sim$ -0.016), however, the number of particles is not enough compared to the width of the histogram to allow a quantitative comparison of our single-particle measurements with the ensemble measurement. It should be noted here that at the moment the optical measurements were performed we did not realize, and therefore did not record, all the parameters that were necessary to determine an absolute sign of our CD measurements. That means that we cannot tell whether a negative/positive CD signal refers to more absorption of left- or more absorption of right-circularly polarized light. However, it should also be noted that the measurements are sign-consistent within themselves meaning that all particles that shows a certain sign in the CD measurement, all absorb either more left- or more right-circularly polarized light. Even though we cannot relate the sign of the CD measurements to whether the particles absorb more left or more right circularly polarized light, our first finding, that the particles' CD is broadly distributed with particles having both positive and negative chiroptical response still holds true. We chose the sign such that it is in agreement with the ensemble measurements in figure S4.1.

A direct comparison with the ensemble measurements is anyway only partially justified as the PT measurements are carried out for particles lying flat on the surface while the CD values obtained by the CD spectrometer, being measured in solution, averages the response of particle orientations. Different particle orientations can affect the chiroptical response. Furthermore, larger nanoparticles, especially rod-like ones, can have a scattering contribution to the extinction signal, that can be on the order of the absorption [2] contribution. Therefore we cannot neglect possible contributions due to circular dichroism scattering of the ensemble measurements which measures a combination of scattering and absorption.

We then take a closer look at the 7 nanorods on which we performed ET measurements to reconstruct their 3D shape. The left sides in figure 4.2 (a), (d), (g) show the 3D visualization of ET results of three nanorods with significantly different g-factors, from a highly chiral nanorod with a positive g-factor (a) to a nanorod with an one order of magnitude lower g-factor (d) and a nanorod with negative g-factor (g). González-Rubio et al. [13], who performed ET studies on particles grown by the same method, concluded that the chiroptical signal of these nanorods stem from helical features in their morphology. Consequently, we tracked local helical features for our correlated morphologies based on the geometrical shape obtained from the reconstruction. Details about the procedure can be found in section 4.4. In short, after converting the reconstruction to cylindrical coordinates, all pixels in the corresponding FFT with the same orientation are binned. The quantification of the directionality can then be used to quantify the helicity. The right sides of figure 4.2 (a), (d), (g) shows the calculated helical features overlaid with the thresholded reconstructions. Interestingly, it becomes immediately clear that each particle contains both, left- and right-handed features.

To further quantify the helicity, we projected the reconstructions in cylindrical coordinates along the radius. The results are shown in figure 4.2 (b), (e), (h). Based on the projections, we created helicity maps as shown in (c), (f) and (i). The mix of helicities within each particle becomes immediately clear in the projected maps as well. Yet, there are also clear

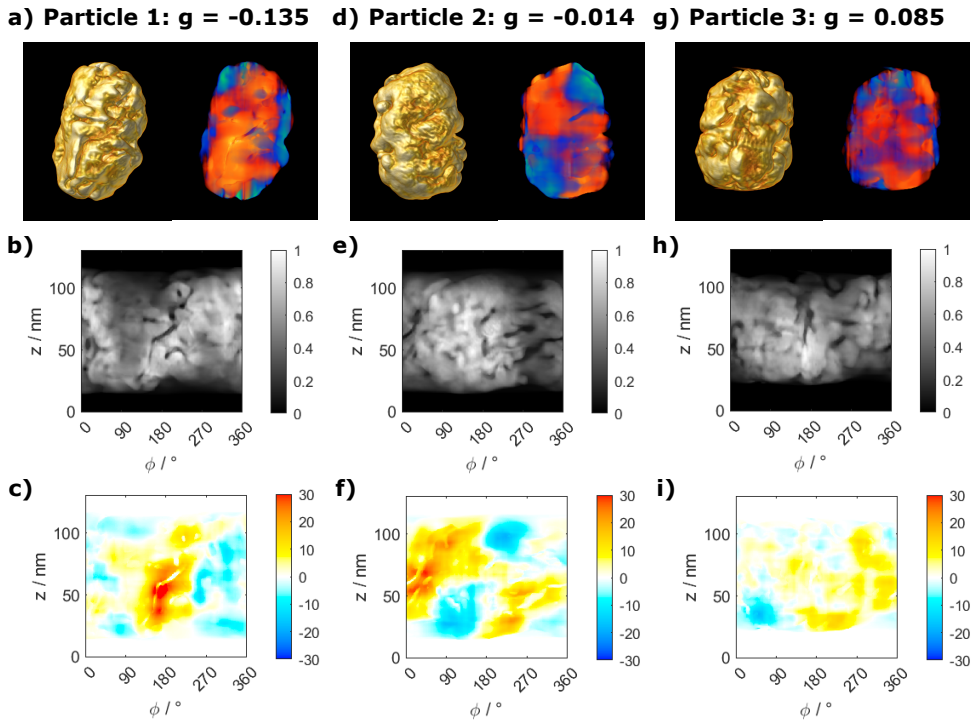

Figure 4.2: Correlation of measured g-factors and electron tomography on single chiral nanorods. (a), (d), (g) show 3D visualizations (left) of three nanorods with different g-factors, which were measured by single-particle PT-CD. The right images show local geometrical helicities of the same nanorods. Red and blue colors correspond to positive and negative helicities. (b), (e), (h) display the radially projected and unwrapped nanorods. (c), (f), (i) show the radially projected helicity maps.

differences between the three particles. The nanorod in (a) with a strong positive g-factor exhibits a prominent area of strong positive geometrical handedness as shown in red in figure (c). This strong chiral feature is related to the big groove around 200° in (b), and is also visible in the 3D visualization in (a). It seems to dominate the overall optical response leading to the high positive g-factor. For the nanorod with one order of magnitude lower g-factor, the projected helicity map in (f) shows areas of relatively strong positive handedness but also large regions of opposite handedness. It seems that the areas of different handedness average out the optical chirality to some extent leading to a much lower g-factor compared to particle 1. Particle 3, for which we measured a strong negative g-factor, displays only areas with weak positive and weak negative geometrical helicity (figure 4.2(i)). From the "helical-like" geometrical features, that were assigned by González-Rubio et al. [13] to be responsible for the chiroptical response, it is thus not conclusive where the negative g-factor stems from.

Figure 4.3 presents the average of the projected helicity maps as a function of the measured g-factor for 7 particles including the ones from figure 4.2. For 6 out of the 7 nanorods that we measured, a positive g-factor correlated to a positive average helicity. This corre-

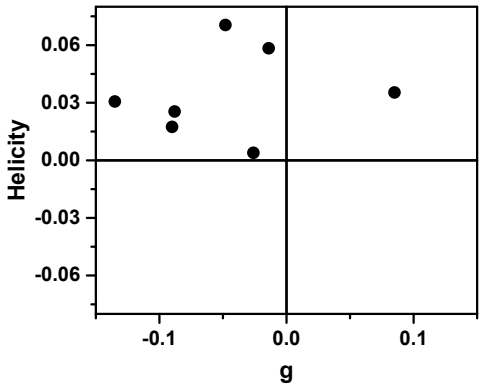

Figure 4.3: Average of helicity maps as a function of measured g-factor for 7 single nanorods.

lation indicates that the average geometrical chirality is indeed influencing the chiroptical properties.

The important conclusion from figure 4.3 is that the strength of the CD signal cannot be directly connected to the average helicity, meaning that stronger geometrical chiral features do not necessarily lead to a stronger chiroptical response. Consequently, additional factors must significantly influence the optical response. On the one hand, of course, plasmonic effects play a role. Due to the differences in shape, each nanorod has a different plasmonic resonance. However, it is quite challenging to perform simulations to understand the plasmonic effect on the chiroptical behavior of a chiral nanorods because of its complex structure. We rather chose a much simpler geometry such as quasi-spherical gold nanoparticles to get a better understanding of the relation between geometrical features and plasmonic influence with their optical CD properties, which we discuss in the following section.

4.2.2. Nominally achiral nanoparticles

To elucidate what other effects play a role, we looked at quasi-spherical gold nanoparticles. We chose for Au truncated octahedra as they are known to be single-crystalline, which avoids any influences from crystalline defects. These gold nanoparticles are often considered as being "achiral". However, due to their wet-chemical synthesis they are heterogeneous in size and shape. Like with the chiral nanorods we performed correlated optical and ET measurements to obtain the optical CD g-factors as well as the structural information of the quasi-achiral particles. Figure 4.4 shows correlative optical and tomography images of four single gold nanoparticles. Figure 4.4 (a) and (b) show PT and PT-CD images and figure (c) shows tomography images of the same four particles. The PT signal, which scales linearly with the absorption, shows different absorption strength, which is normally related to different sizes of the particles. In this case, however, the topology of the substrate surface of the TEM grid-window causes some particles to be either in- and others to be out-of-focus within one scan area. To determine the CD of the particles we calculate their g-factor, which is defined as the differential absorption divided by the total (isotropic) absorption. As we

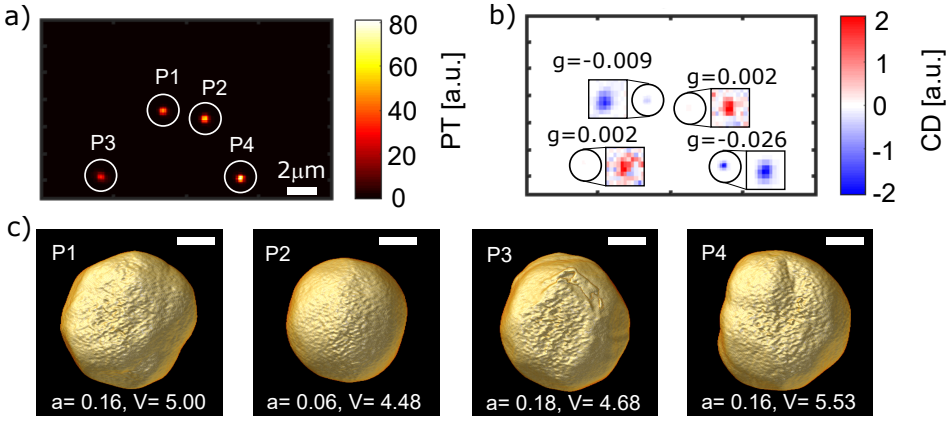

Figure 4.4: (a) PT and (b) PT-CD images of four single gold nanoparticles. Solid circles are drawn to show correlation between the two images. To show the contrast of the weak signals in CD, each particle's image in (b) is shown with an adjusted contrast as marked with square boxes. The numbers in (b) correspond to the particle's g-factor. The scale bar in (a) is $2\,\mu\mathrm{m}$. (c) Electron tomography of the four single-particles as labelled in (a). The scale bar is $30\,\mathrm{nm}$. In (c) a is the asphericity and V is the volume of the particle in nm^3 divided by factor of 10^5.

show in figure S4.2, defocusing affects both the PT and the CD measurements alike and therefore the g-factor is independent of the focus position.

The 3D reconstructed images of the single-particles, displayed in figure 4.4 (c), show that the particles are heterogeneous in shape. We use the reconstructed images to calculate the particles' asphericity. The asphericity is as a measure of the deviation from a spherical shape. An asphericity equal to 0 corresponds to a perfect sphere and for a non-spherical shape asphericity is greater than 0. The inset in figure 4.4 (c) indicates the respective asphericity of the particles. Particle P2 has a low asphericity and exhibits a weak g-factor of 0.002, on the other hand, particles with large asphericity (P1, P3 and P4) can exhibit both strong and weak CD signals. In the optical measurements we only probe one specific orientation of the geometry and therefore are not sensitive to deviations from the spherical shape along the optical axis. When we calculate the asphericity from the shape we therefore have to neglect protrusions of the particle along the optical axis, this is indicated by the "2D".

In total we have measured 25 single gold nanoparticles correlated with tomography measurements. Figure 4.5 (a) shows the correlation between asphericity and measured g-factors. We find that particles with low asphericity mostly exhibit weak CD signals while particles with higher asphericity can exhibit both, strong and weak CD signals. We conclude that asphericity is needed to create CD but asphericity does not inevitably lead to CD. A nanorod for example would have nonzero asphericity but clearly is not chiral. A more meaningful measure to represent geometric chirality than asphericity is the Hausdorff chirality which is a measure of the lack of congruence of an object with its mirror image [14]. It measures the missing volumetric overlap of an object with its mirror image. A rod-shaped object, which is achiral, will have zero Hausdorff chirality, whereas it will have nonzero asphericity. Figure 4.5 (b) shows the correlation between Hausdorff chirality and the optical CD measurements. As we probe only a specific orientation of the particle we must calculate the Hausdorff chi-

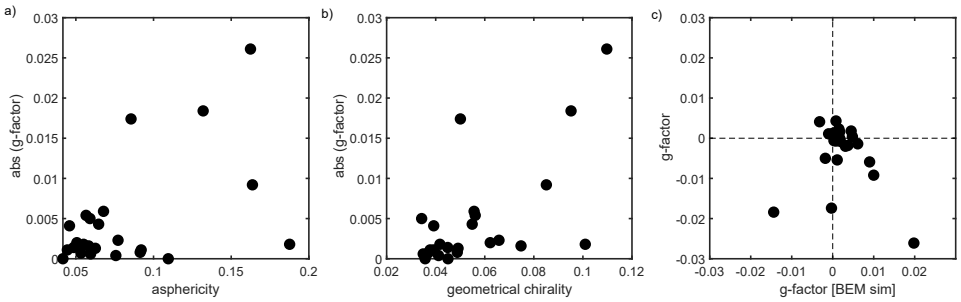

Figure 4.5: Correlation plots of g-factor obtained from the experiment with (a) 2D-asphericity, (b) 2D Hausdorff and (b) g-factor calculated with the boundary element method (BEM) simulation at $532\,\mathrm{nm}$. None of the correlation plots show a direct correlation between the corresponding parameters for all particles.

rality using only rotations along the optical axis and translations perpendicular to it which is indicated by the "2D". We find that smaller 2D Hausdorff chirality values correlate with smaller g-factors, and that larger Hausdorff values allows for but do not guarantee large g-factors. Compared to the asphericity measure we find a better correlation for the Hausdorff chirality with the optical measurements, but from our purely geometric considerations we again can conclude that there is a fundamental difference between the geometric-chirality of an object and its optical manifestation at a given wavelength (here the CD at $532\,\mathrm{nm}$).

Besides the fact that the wavelength plays an important role, plasmonic effects can also enhance CD. Such behaviour cannot be predicted by geometric considerations alone. We therefore also performed BEM simulations of the same 25 ET-reconstructed particles. Figure 4.5 (c) shows the correlation between optical measurements and BEM simulations using the Matlab MNPBEM toolbox. As opposed to asphericity and Hausdorff chirality we can also take into account the sign of the CD signal. Most of the particles that have weak CD values (below a g-factor of 0.01) also exhibit a weak CD in the optical measurements and simulations. However, for particles with larger optical CD values we also find cases with substantial deviations from the BEM simulations. One particle for example has strong negative CD for both optical measurements and BEM, other particles though have strong CD effects with opposite sign in experiment and simulations. Here we must note again that we missed to record all the necessary parameters to be able to tell whether a positive/negative sign in the CD measurements corresponds to more absorption of left or right circularly polarized light. The correlation plot in figure 4.4 (c) therefore shows an arbitrarily chosen sign for the CD measurements. However, the absence of a clear correlation of BEM calculations and CD measurements persists in both cases.

We think that there might be additional effects, which contribute to the particles' CD signal but that are not related to the particles' shape, and therefore lead to the mismatch of optical measurements and the simulations based on the reconstructed geometry. We hypothesize several sources that could contribute to the CD signal. First of all the substrate will have an influence on the chiroptical response as has been shown earlier [15, 16]. Even though we use immersion-oil for the optical measurements, which should match the substrate's refractive index, as we heat the oil during the measurement we effectively decrease its refractive index. Additionally, the substrate (silica) on which the particles reside is only

18 nm thick and we cannot exclude the presence of an air cavity behind the substrate's surface. An air cavity behind a very thin substrate could additionally introduce a symmetry break [15], due to the refractive index mismatch. Furthermore, we imagine that ligands on the nanoparticle's surface could play a role as well as they have been reported to alter the particle's plasmonic response [17].

4.3. Conclusion

The synthesis process of chiral nanorods creates a weak bias towards a certain geometric handedness as well as the chiroptical response of the particles, when measurements are performed on a large ensemble of particles in solution. However, the study of individual particles revealed that the strength of the chiroptical response is not directly related to the helicity as particles with a large helicity can have weak chiroptical response and vice versa. This may be related to plasmonic effects, however, as we show with our simple model-system of quasi achiral particles, even plasmonic effects cannot satisfactorily explain the relation between shape and chiroptical response. That means that, even if we knew the shape of a nanoparticle and were able to simulate its chiroptical response, thereby taking into account also its plasmonic behaviour (and wavelength dependence), we find only a weak correlation between measurement and simulations and thus the geometry. Other effects that we have not taken into account may add a residual CD signal that do not allow us to determine the optical response if we consider only the geometry of the particle. Such effects might be related to surface ligands, or the substrate which can cause an additional symmetry break and therefore alter the chiroptical response of nanoparticles. Due to the broad distribution of g-factors in chemically-synthesized nanoparticles, more measurements would be necessary to draw concrete conclusions. Furthermore we should make sure to determine the global sign of the optically measured CD signal to allow for a direct comparison of BEM simulations and optical measurements.

4.4. Experimental

4.4.1. Sample preparation

For the correlative transmission electron microscopy and optical measurement, single gold nanospheres (diameter of 100 nm, purchased from nanoComposix) or single chiral gold nanorods (wet chemically-synthesized according to reference [13]) were drop-casted on a TEM grid which contains silicon dioxide support film of thickness 18 nm and aperture of $70 \times 70\,\mu m^2$ (product no.: 21532-10, purchased from Ted Pella). The TEM grid was then sandwiched with a second glass slide (thickness of about 170 µm). An immersion oil was used as a photothermal medium because of its high viscosity and hydrophobicity which was essential for the sandwiched TEM grid sample. For measurements of single gold nanospheres, immersion oil of refractive index of 1.51 and for measurements of single chiral gold nanorods, an immersion liquid of refractive index of 1.33 were used. First optical measurements were performed and thereafter the TEM grid was cleaned with toluene to remove the immersion oil. The cleaned TEM grid containing single gold nanospheres was used for TEM measurements. For optical measurements only the nanospheres or nanorods which

were deposited on the marked silicon dioxide windows, were chosen. TEM measurements were performed on the same nanospheres or nanorods. For nanorods and nanospheres measurements, the heating laser powers were $25.6\,\mathrm{mW}$ and $8\,\mathrm{mW}$, respectively illuminated in an area of about $20\,\mu\mathrm{m}^2$ and the probe laser powers were $0.8\,\mathrm{mW}$ and $2\,\mathrm{mW}$, respectively in a diffraction-limited focus area.

4.4.2. g-factor analysis of optical measurements

g-factors were calculated as the ratio of mean values of photothermal and photothermal circular dichroism signal averaging in an area of 7×7 pixels^2 around the centroid position of each individual particle.

4.4.3. Transmission electron microscopy and tomography

HAADF-STEM images and electron tomography tilt series were acquired using a FEI-Osiris electron microscope operated at $200\,\mathrm{kV}$. Tilt series were acquired for the maximal possible tilt range for the SiO_2 TEM grids, which was generally around $\pm65°$. The tilt increment was 3°. The tilt series for the achiral nanoparticles were reconstructed in the following manner: After aligning the tilt series images by cross-correlation, the stacks of aligned projection images served as inputs for 100 iterations of the expectation maximization implemented in the ASTRA toolbox [18, 19]. The reconstructions were furthermore thresholded using the Otsu method and the thresholded reconstructions were used for determining the volume. The tilt series for the more complex chiral nanorods were reconstructed in the following manner: After distortion corrections with the help of a convolutional neural network, 3D reconstructions were performed by the simultaneous iterative reconstruction technique and the application of constraints in real and Fourier space, following previous work [13].

4.4.4. Quantification of asphericity

The asphericity is a metric used to determine how much a given shape differs from a sphere. To calculate this metric, we segmented the 3D ET reconstructions to retrieve a binary volume. We then calculated the volume of the reconstructed shape and created a new binary volume containing a perfect sphere with the same volume. The asphericity was then calculated as the minimal shape error between the reconstructed volume and the sphere.

4.4.5. Hausdorff chirality quantification

The Hausdorff chirality measure is a measure to quantify the chirality of a set of points which typically describe a molecule. This chirality measure is determined by calculating the minimum Hausdorff distance between a set of points and the mirror image of that set of points. To make the measure scale-invariant, the result is then divided by the diameter of this set of points, which is calculated as the maximum distance between any two points of the set. However, since our data is stored as a 3D volume, we adapted the Hausdorff method as follows and call it as geometrical chirality. First the 3D ET reconstructions were segmented into binary volumes. Next, analogously to the Hausdorff chirality measure, we

define a chirality measure as the minimum shape error between the binary reconstruction and its mirror image. The shape error is defined as the number of mismatching voxels divided by the number of voxels included in the volume and is therefore already scale-invariant. The chirality measure is found by minimizing the shape error for rigid transformations of the mirrored volume.

4.4.6. Boundary element method simulations

The discretized Otsu thresholded tomography reconstructions of the Au nanoparticles served as an input for BEM calculations, which were performed solving the full Maxwell equations at 100 points in the wavelength range from 500 to 700 nm using left and right circularly polarized light using the MNPBEM Matlab toolbox v17. The g-factor was then determined as defined in chapter 2.

4.4.7. Quantification of helicity

Helicity can be quantified by investigating the directionality of features in a three-dimensional volume in cylindrical coordinates. Namely, features that are oriented parallel with the (x, y)-plane (horizontal) or with the z-axis (vertical) can be labeled as being "achiral", while other features are oriented such that they wrap around the z-axis and are therefore helical. To quantify this, we calculated the local helicity for each voxel in cylindrical coordinates by investigating the directionality of a small region around that voxel in the (ϕ, z)-plane according to the method described in [20], which uses the gradient to quantify the local helicity in a region. More specifically, features of a particle will show a strong change in intensity in the direction orthogonal to the inclination angle. For example, horizontal features correspond to a wavevector parallel to $\vec{g} = (0, g_z)$ and vertical features correspond to a wavevector parallel to $\vec{g} = (g_\phi, 0)$. Right-handed features will be represented by $\vec{g} = (g_\phi, g_z)$ with $g_z \cdot g_\phi < 0$ and left-handed features analogously by $\vec{g} = (g_\phi, g_z)$ with $g_z \cdot g_\phi > 0$. This insight leads to a filter that can be used for the quantification of helicity:

$$H(g_\phi, g_z) = -sign(g_\phi \cdot g_z) \tag{4.1}$$

with

$$sign(x) = \begin{cases} -1, x < 0 \\ 1, x > 0 \\ 0, x = 0 \end{cases} \tag{4.2}$$

The local helicity in a voxel at location (ρ_i, ϕ_i, z_k) is then given by

$$H(\rho_i, \phi_i, z_k) = \iint dk_\phi dk_z \|\vec{g}\| \cdot H, \tag{4.3}$$

where $\vec{g}$ is the magnitude of the gradient at a given location and the integral goes over a small two-dimensional window around the (ρ_i, ϕ_i, z_k) voxel in the (ϕ, z)-plane. The magnitude of the gradient is taken as a metric that indicates the "amount" of features oriented in a certain direction. For our experiments, we used windows of 64×64 pixels. This method results

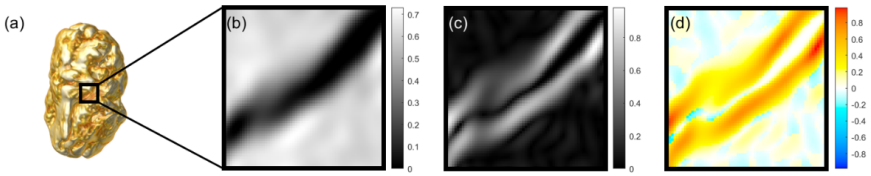

Figure 4.6: The procedure to calculate the helicity measure in a small region of the volume. A 3D rendering of one of the chiral nanorods is shown in (a), a small region around a voxel is selected in (b), the magnitude of the gradient is shown in (c), and the orientation of the gradient is used to assign the correct sign indicating the handedness to each pixel as shown in (d).

in a single value for each voxel in cylindrical coordinates that indicates the helicity of the particle in that region. Positive values correspond to right-handed helicity and negative values to left-handed helicity. Figure 4.6 illustrates this procedure: (a, b) select a region in a slice around a voxel from the 3D volume, (c) calculate the gradient of this region and (d) apply the H filter. The helicity value for the selected voxel is the sum over the result in (d), which is in this case positive and therefore indicates that the feature is right-handed.

4.5. Supplementary information

4.5.1. Ensemble CD spectra of the S-enantiomer of chiral nanorods

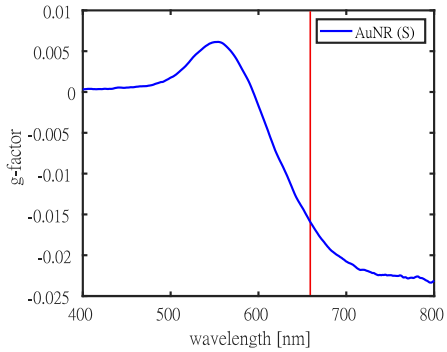

Figure S4.1: Ensemble circular dichroism (CD) spectra of an aqueous solution of chiral gold nanorods with S enantiomers. The g-factor at 660 nm indicated by the vertical red line is about -0.016.

Figure S4.1 shows a CD spectrum of a diluted stock solution of the chiral nanorods obtained by a commercial CD spectrometer. Our optical single-particle CD measurements were carried out at 660 nm as indicated by the vertical red line. At that wavelength the ensemble measurements yields a g-factor of -0.016.

4.5.2. Effect of defocusing on the CD g-factor

Because of the non-flat surface of the TEM grid window, some particles are in-focus and others are slightly out-of-focus in our optical measurements. Therefore, we checked if the slight defocusing may have an influence on the CD g-factor. We measured a single 100 nm gold nanoparticle in-focus and out-of-focus as shown in figure S4.2. Slight defocusing decreases both photothermal (PT) and circular dichroism (CD) signals alike and therefore the calculated g-factor (i.e. the ratio of CD and PT) remains nearly unchanged.

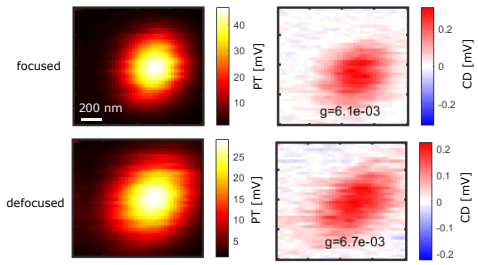

Figure S4.2: Photothermal (PT) and circular dichroism (CD) image of a single gold nanoparticle in (a) focused and (b) slightly defocused conditions showing slight defocusing has nearly no influence in the value of g-factor.

References

[1] Vinegrad, E.; Vestler, D.; Ben-Moshe, A.; Barnea, A. R.; Markovich, G.; Cheshnovsky, O. Circular Dichroism of Single Particles. *ACS Photonics* **2018**, *5*, 2151–2159.

[2] Wang, L. Y.; Smith, K. W.; Dominguez-Medina, S.; Moody, N.; Olson, J. M.; Zhang, H.; Chang, W. S.; Kotov, N.; Link, S. Circular Differential Scattering of Single Chiral Self-Assembled Gold Nanorod Dimers. *ACS Photonics* **2015**, *2*, 1602–1610.

[3] Lu, X.; Wu, J.; Zhu, Q.; Zhao, J.; Wang, Q.; Zhan, L.; Ni, W. Circular Dichroism From Single Plasmonic Nanostructures With Extrinsic Chirality. *Nanoscale* **2014**, *6*, 14244–14253.

[4] Zhang, Q.; Hernandez, T.; Smith, K. W.; Jebeli, S. A. H.; Dai, A. X.; Warning, L.; Baiyasi, R.; McCarthy, L. A.; Guo, H.; Chen, D.-H., et al. Unraveling the Origin of Chirality From Plasmonic Nanoparticle-Protein Complexes. *Science* **2019**, *365*, 1475–1478.

[5] Spaeth, P.; Adhikari, S.; Le, L.; Jollans, T.; Pud, S.; Albrecht, W.; Bauer, T.; Caldarola, M.; Kuipers, L.; Orrit, M. Circular dichroism measurement of single metal nanoparticles using photothermal imaging. *Nano Letters* **2019**, *19*, 8934–8940.

[6] Spaeth, P.; Adhikari, S.; Baaske, M. D.; Pud, S.; Ton, J.; Orrit, M. Photothermal Circular Dichroism of Single Nanoparticles Rejecting Linear Dichroism by Dual Modulation. *ACS Nano* **2021**,

[7] Gansel, J. K.; Thiel, M.; Rill, M. S.; Decker, M.; Bade, K.; Saile, V.; von Freymann, G.; Linden, S.; Wegener, M. Gold Helix Photonic Metamaterial as Broadband Circular Polarizer. *Science* **2009**, *325*, 1513–1515.

[8] Hendry, E.; Carpy, T.; Johnston, J.; Popland, M.; Mikhaylovskiy, R.; Lapthorn, A.; Kelly, S.; Barron, L.; Gadegaard, N.; Kadodwala, M. Ultrasensitive Detection and Characterization of Biomolecules Using Superchiral Fields. *Nature Nanotechnology* **2010**, *5*, 783–787.

[9] Coles, R.; Price, D.; Dixon, J.; Royall, B.; Clarke, E.; Kok, P.; Skolnick, M.; Fox, A.; Makhonin, M. Chirality of Nanophotonic Waveguide With Embedded Quantum Emitter for Unidirectional Spin Transfer. *Nature Communications* **2016**, *7*, 1–7.

[10] Pendry, J. A Chiral Route to Negative Refraction. *Science* **2004**, *306*, 1353–1355.

[11] Hentschel, M.; Schäferling, M.; Duan, X.; Giessen, H.; Liu, N. Chiral Plasmonics. *Science Advances* **2017**, *3*, e1602735.

[12] Kusar, P.; Gruber, C.; Hohenau, A.; Krenn, J. R. Measurement and Reduction of Damping in Plasmonic Nanowires. *Nano Letters* **2012**, *12*, 661–665.

[13] González-Rubio, G.; Mosquera, J.; Kumar, V.; Pedrazo-Tardajos, A.; Llombart, P.; Solís, D. M.; Lobato, I.; Noya, E. G.; Guerrero-Martínez, A.; Taboada, J. M.; Obelleiro, F.; MacDowell, L. G.; Bals, S.; Liz-Marzán, L. M. Micelle-Directed Chiral Seeded Growth on Anisotropic Gold Nanocrystals. *Science* **2020**, *368*, 1472–1477.

[14] Buda, A. B.; Mislow, K. A Hausdorff Chirality Measure. *Journal of the American Chemical Society* **1992**, *114*, 6006–6012.

[15] Nechayev, S.; Barczyk, R.; Mick, U.; Banzer, P. Substrate-Induced Chirality in an Individual Nanostructure. *ACS Photonics* **2019**, *6*, 1876–1881.

[16] Arteaga, O.; Sancho-Parramon, J.; Nichols, S.; Maoz, B. M.; Canillas, A.; Bosch, S.; Markovich, G.; Kahr, B. Relation Between 2D/3D Chirality and the Appearance of Chiroptical Effects in Real Nanostructures. *Optics Express* **2016**, *24*, 2242.

[17] Ghosh, S. K.; Nath, S.; Kundu, S.; Esumi, K.; Pal, T. Solvent and Ligand Effects on the Localized Surface Plasmon Resonance (LSPR) of Gold Colloids. *The Journal of Physical Chemistry B* **2004**, *108*, 13963–13971.

[18] Moon, T. K. The Expectation-Maximization Algorithm. *IEEE Signal Processing Magazine* **1996**, *13*, 47–60.

[19] Van Aarle, W.; Palenstijn, W. J.; De Beenhouwer, J.; Altantzis, T.; Bals, S.; Batenburg, K. J.; Sijbers, J. The ASTRA Toolbox: A Platform for Advanced Algorithm Development in Electron Tomography. *Ultramicroscopy* **2015**, *157*, 35–47.

[20] Heyvaert, W.; Pedrazo-Tardajos, A.; Kadu, A.; Claes, N.; González-Rubio, G.; Liz-Marzán, L. M.; Albrecht, W.; Bals, S. Quantification of the helical morphology of chiral Au nanorods. 2022.